Journal of Materials Chemistry C

Controlling the threshold voltage of β-Ga_2O_3 field-effect transistors *via* remote fluorine plasma treatment

Journal:	*Journal of Materials Chemistry C*
Manuscript ID	TC-ART-05-2019-002468.R1
Article Type:	Paper
Date Submitted by the Author:	13-Jun-2019
Complete List of Authors:	Kim, Janghyuk; Korea University, Tadjer , Marko ; US Naval Research Laboratory Mastro, Michael; US Naval Research Laboratory, Kim, Jihyun; Korea University, Department of Chemical and Biological Engineering

Controlling the threshold voltage of β-Ga_2O_3 field-effect transistors *via* remote fluorine plasma treatment

Janghyuk Kim[†], Marko J. Tadjer[‡], Michael A. Mastro[‡] and Jihyun Kim[†,*]

[†]Department of Chemical and Biological Engineering, Korea University, Seoul 02841 Korea

[‡]US Naval Research Laboratory, 4555 Overlook Ave. SW, Washington, DC 20375 USA

ABSTRACT

β-phase gallium oxide (β-Ga_2O_3), emerging as an ultra-wide bandgap semiconductor, suffers from negative threshold voltage (V_{th}) characteristics, which only allow depletion-mode (D-mode) operation; however, enhancement-mode (E-mode) operation is preferred to ensure fail-safe operation and simplify circuit topologies. Therefore, in this study, the V_{th} is controlled via remote fluorine plasma treatment in β-Ga_2O_3 metal-insulator-semiconductor field-effect transistors (MISFETs). Under the top-gate modulation, the V_{th} of the fluorinated β-Ga_2O_3 MISFET was positively shifted by +4 V, exhibiting high on/off ratio (~10^7) and low sub-threshold swing (175 mV/dec). Under the double-gate modulation, the E-mode β-Ga_2O_3 MISFET was demonstrated, where the V_{th} was estimated to be +2.2 V. The obtained results suggest that the fluorine plasma treatment is an effective method to control the V_{th} of the β-Ga_2O_3 FETs from D-mode to E-mode, pointing out monolithic integration of β-Ga_2O_3 transistors for future smart power electronics.

KEYWORDS: gallium oxide; field-effect transistors; enhancement-mode; plasma treatment

***Corresponding Author:** E-mail: hyunhyun7@korea.ac.kr (Jihyun Kim)

INTRODUCTION

β-phase gallium oxide (β-Ga_2O_3) is a promising semiconductor material for next-generation high-power electronics because of its ultra-large energy bandgap of 4.8 eV (room temperature) and a theoretical critical field strength of approximately 8 MV/cm.[1–3] The Baliga's figure of merit,[4] which is the metric of conduction loss in power devices, of β-Ga_2O_3 (at 3214) is considerably higher than those of SiC (at 317) and GaN (at 846). This indicates that β-Ga_2O_3-based power electronics are more efficient than other competing wide bandgap materials. As the proportion of electrical energy passing through power electronics has been increasing considerably, near-future power electronics utilizing β-Ga_2O_3 as an active layer can lead to a considerable reduction in energy consumed. [5] Furthermore, another prominent feature of β-Ga_2O_3 compared to other wide-bandgap semiconductors is that high-quality single crystals can be synthesized cost-effectively using melt growth techniques such as the floating zone, Czochralski and edge-defined film-fed growth. Therefore, it can be concluded that β-Ga_2O_3 has an economical advantage over SiC and GaN.

β-Ga_2O_3 device technology has developed rapidly in recent years and various transistors, including MOSFETs, MESFETs, and FinFETs, have been successfully demonstrated. Higashiwaki et al. pioneered single-crystal β-Ga_2O_3-based transistors.[6] Tadjer et al. demonstrated a β-Ga_2O_3 MOSFET with HfO_2 gate dielectric layer.[7] Interestingly, a single crystalline β-Ga_2O_3 with a monoclinic structure can be exfoliated into ultra-thin flakes along a (100) plane owing to its strong in-plane force and weak out-of-plane force,[8-10] demonstrating various β-Ga_2O_3 nano-layer based transistors.[10–13] β-Ga_2O_3 typically contains oxygen vacancies, and therefore, β-Ga_2O_3 has been considered as an n-type semiconductor.[14] Recently, it is reported that the oxygen vacancy cannot contribute to the conductivity because they are deep donors.[15] Furthermore, n-type dopants including Si and Sn have been incorporated to achieve higher carrier concentrations.[2] Therefore, most of the fabricated β-

Ga_2O_3 transistors exhibit n-type characteristics with a negative threshold voltage (V_{th}).[6,12,16,17] The negative V_{th} of n-type β-Ga_2O_3 transistors allows only depletion mode (D-mode) operation, which limits their implementations in electronic circuits. Enhancement-mode (E-mode) operation is preferred for power transistors, which enables simple circuit designs and fail-safe operation under high voltage conditions.[18,19]

Various techniques have been suggested to control V_{th}, including forming trench- or Fin-shaped channels,[20,21] partial Si doping,[22] and thickness control of β-Ga_2O_3 channel.[23] In addition, incorporating fluorine close to the channel is an efficient method to modulate the V_{th} of FETs. Fluorine plasma treatment has been previously used to control the V_{th} of AlGaN/GaN high electron mobility transistors (HEMTs) and amorphous InGaZnO (a-IGZO) thin-film transistors.[24–28] The incorporated fluorine atoms, which have high electronegativity, are negatively charged and increase the potential in the AlGaN or a-IGZO barrier, which results in a positive shift of V_{th}. Yang et al. reported that when the fluorine plasma was exposed, the barrier height of β-Ga_2O_3 Schottky barrier diodes was increased; this was because the Si donors were compensated by fluorine atoms, forming neutral complexes.[29] In this work, we demonstrate a facile, efficient, and reproducible method to control the V_{th} of β-Ga_2O_3-based metal insulator field-effect transistors (MISFETs) via remote CF_4 plasma treatment. E-mode operation was achieved under the double gate condition, presenting a potential for β-Ga_2O_3-based smart power integrated circuit (IC) applications.

EXPERIMENTAL DETAILS

Two MISFETs in series were fabricated on a single β-Ga_2O_3 flake. Figures 1(a–d) show optical microscope images that present the fabrication sequence of pristine and fluorinated β-Ga_2O_3 MISFETs on a single flake. β-Ga_2O_3 flakes were obtained from a (-201) β-Ga_2O_3 single crystal by a mechanical exfoliation process. The β-Ga_2O_3 single crystal, which is unintentionally n-doped with an effective carrier density (N_d-N_a) of approximately $3x10^{17}$ cm^{-3}, was produced by the edge-defined film-fed method (Tamura Corp.). Exfoliated β-Ga_2O_3 flakes were then dry-transferred onto a SiO_2 (300 nm)/p^{++}–Si (500 μm) substrate, which was pre-patterned with Ti/Au (20 nm/80 nm) as a bottom-gate electrode (Fig. 1(a)). Source and drain electrodes (Ti/Au 20 nm/80 nm) were defined using an electron-beam (e-beam) lithography and lift-off process (Fig. 1(b)). The channel length and width of β-Ga_2O_3 FETs were 20 μm and 4 μm, respectively. Rapid thermal annealing in an argon atmosphere was performed for 60 sec at 480 °C to form ohmic contact with the exfoliated β-Ga_2O_3 flake. As shown, part of the channel (red box) was opened to the CF_4 plasma treatment by an e-beam lithography after the sample was coated with the electron-beam resist (Fig. 1(c)). The CF_4 plasma was introduced to the surface of the β-Ga_2O_3 flake using a conventional reactive ion etching (RIE) system (RIE 5000, SNTEK). To avoid damage by direct ion bombardment, the sample was placed face-down between the high supports in the RIE chamber, which is similar to the remote plasma configuration. The precursor gas used was CF_4 (50 sccm) at the pressure of 3 mTorr, and the etching power and time were 100 W and 60 sec, respectively. Multilayer h-BN nanosheets were mechanically exfoliated from a bulk powder (Momentive Corp.) and were dry-transferred onto the β-Ga_2O_3 flake. Two h-BN flakes were deposited as a gate dielectric layer. The top gate electrode was defined by depositing Pt/Au (20/80 nm) after e-beam lithography (Fig. 1(d)). A schematic of the fabricated β-Ga_2O_3 MISFETs on a single flake is shown in Fig. 1(e).

The thickness and surface morphology of β-Ga_2O_3 and h-BN were characterized using atomic force microscopy (AFM) (XE100, PSIA). Micro-Raman spectroscopy was conducted with back-scattering geometry using the 532 nm line of a diode-pumped solid-state laser (Omicron) to analyze the structural properties of the exfoliated β-Ga_2O_3 and h-BN layers. X-ray photoelectron spectroscopy (XPS) (Thermo, K-alpha) using the monochromated Al Ka line as the X-ray source was employed to study changes in the bonding structure of the β-Ga_2O_3 flakes after the CF_4 plasma treatment. The electrical and transport characteristics of the fabricated β-Ga_2O_3 MISFETs were obtained using an Agilent 4155C semiconductor parameter analyzer connected to a probe station.

RESULTS AND DISCUSSION

The morphology and thickness of the β-Ga_2O_3 and h-BN nanosheets in the fabricated FETs were analyzed, as shown in Figs. 2(a–b). The β-Ga_2O_3 and h-BN nanosheets were approximately 250 and 25~28 nm thick, respectively. The thickness of the pristine β-Ga_2O_3 was identical to that of the fluorinated one, as shown in Fig. S1, indicating that there was no significant degradation or etching of β-Ga_2O_3 during the remote CF_4 plasma treatment. The crystal quality of the β-Ga_2O_3 flake and h-BN nanosheets was evaluated using micro-Raman spectroscopy (Fig. 2(c)). Phonon peaks corresponding to the β-Ga_2O_3 flake are observed in the range 60–800 cm^{-1}. The peaks near 200, 347, 416, and 767 cm^{-1} correspond to the A_g^3, A_g^5, A_g^6, and A_g^{10} vibration modes of β-Ga_2O_3, respectively.[30,31] The peak at approximately 1350 cm^{-1} corresponds to the E_{2g} vibration mode of h-BN.[32] The Raman spectra also indicate that there was no significant disruption of the sample by remote CF_4 plasma treatment. XPS measurement was performed to investigate the chemical property of the surface of β-Ga_2O_3 flakes after CF_4 plasma treatment. Figure 3(a) shows XPS survey scans of the pristine and CF_4 plasma-treated β-Ga_2O_3, where F1s and F KLL signals appear. A more detailed analysis of the F1s core levels indicates the influence of the CF_4 plasma treatment, where the peak of a

Ga–F bond appears at 684.7 after the CF_4 plasma treatment. This suggests that the remote CF_4 plasma treatment effectively forms a Ga–F bond.[33,34]

Prior to the deposition of the top-gate electrode, the bottom-gated β-Ga_2O_3 FET was characterized to observe the effects of the CF_4 plasma treatment. The I_{DS}–V_{DS} output and transfer characteristics of a bottom-gated β-Ga_2O_3 MOSFET with a thermally grown SiO_2 dielectric, before and after the CF_4 plasma treatment, are compared in Fig. S2 (a–b). After the CF_4 plasma treatment, the V_{th} shifted positively, indicating the F-induced depletion of the channel. The negatively charged fluorine atoms incorporated into the β-Ga_2O_3 partially deplete carriers in the n-channel. For a more detailed analysis of device performance, two h-BN layers as top-gate dielectrics were deposited on top of each channel, making two top-gated MISFETs. Figures 4(a–b) exhibit the I_{DS}–V_{DS} output characteristics of pristine (Fig. 4(a)) and fluorinated (Fig. 4(b)) β-Ga_2O_3-based MISFETs, respectively, both showing good saturation and sharp pinch-off characteristics. The transfer curve for pristine β-Ga_2O_3 top-gated MISFET (Fig. 4(c)) shows a V_{th} of -5.1 V with a current on/off ratio ~10^8 at V_{DS} = +10 V. An estimated field effect carrier mobility (μ_{FE}) and a sub-threshold swing (SS) were about 18.9 cm^2 V^{-1} s^{-1} and 350 mV dec^{-1}, respectively. The μ_{FE} can be obtained from the following equation:

$$\mu_{FE} = \frac{L}{W}\frac{2}{C_g}\left(\frac{\partial\sqrt{I_{DS}}}{\partial V_{TG}}\right)^2$$

, where L and W denote the length and width of the channel, respectively. C_g is the gate dielectric capacitance per unit area, and V_{TG} is the top gate bias. These transfer properties are comparable to previous reports of FETs using unintentionally doped β-Ga_2O_3. For fluorinated β-Ga_2O_3 MISFET, V_{th} of -1.1 V and μ_{FE} of 37.2 cm^2 V^{-1} s^{-1} with a current on/off ratio ~10^7 were extracted at V_{DS} = +10 V, as shown in Fig. 4(c). The SS of fluorinated β-Ga_2O_3 MISFET (~172 mV·dec^{-1}) is lower than that of a pristine β-Ga_2O_3 MISFET, and the gate leakage currents for both pristine and fluorinated β-Ga_2O_3 MISFETs are almost equivalent, implying nominal plasma-induced damage. The positive shift of V_{th} from -5.1 to -1.1 V is observed in fluorinated β-Ga_2O_3 when compared with pristine β-Ga_2O_3 under the top-gate operation, where V_{th} was extracted from the plot of the square root of drain current versus gate voltage. The F atom adsorbed on the β-Ga_2O_3 has a strong electronegativity (3.98), increasing the depletion region in the β-Ga_2O_3 channel. Figure 4(d) shows the energy band diagram of the interface between β-Ga_2O_3 and h-BN before and after the CF_4 plasma treatment. The fluorine atoms on the surface increased the $V_{th}(= \psi_{bi} - \psi_P)$ by lowering the pinch-off potential ($\psi_P = \frac{qN_Dd^2}{2\varepsilon_s}$), where ψ_{bi}, q, N_D, d and ε_s are the built-in potential, electronic charge, carrier concentrations, channel height, and the channel material's permittivity, respectively.[35] The edge of the conduction band of fluorinated β-Ga_2O_3 at the interface between β-Ga_2O_3 and h-BN bends upward, and the depletion width extends.

Double gate operation of pristine and fluorinated β-Ga_2O_3 MISFETs was performed, sweeping top-gate bias with varying bottom gate (V_{BG}) bias as shown in Fig. 5. V_{th} of the pristine β-Ga_2O_3 MISFET shifted from -5.1 V to -3.1 V as the V_{BG} varied from 0 to -9 V. Meanwhile, V_{th} of the fluorinated β-Ga_2O_3 MISFET gradually shifted from -1.1 V to +2.2 V, demonstrating an E-mode operation. As shown in Fig. 5(c), the incorporation of F into the top surface facilitated the positive V_{th} under the double gate operation. The formation of an E-mode MISFET and a D-mode MISFET in the single β-Ga_2O_3 flake via partial the CF_4 plasma treatment can be utilized to fabricate various circuit designs. Our approach allows the fabrication of E-mode β-Ga_2O_3 FETs as well as the monolithic integration of E/D-mode FETs, both of which are expected to give valuable circuit applications, such as logic inverters.[36] These results suggest that the CF_4 plasma treatment, which is controllable and compatible with the CMOS process, provides a simple approach to achieve V_{th} control of β-Ga_2O_3 FETs, proposing β-Ga_2O_3-based logic devices for future miniaturized smart power and harsh environment electronics.

CONCLUSION

The V_{th} of β-Ga_2O_3 FETs was controlled from D-mode to E-mode through the remote CF_4 plasma treatment, demonstrating a β-Ga_2O_3-based E/D-mode FETs in a single β-Ga_2O_3 flake. The V_{th} was positively shifted by +4 V compared with a pristine β-Ga_2O_3 FET owing to the incorporated fluorine atoms with high electronegativity. A Ga–F bond was formed on β-Ga_2O_3 using the remote CF_4 plasma treatment. The fluorinated β-Ga_2O_3 MISFET displayed excellent transistor characteristics with I_{DS} on/off ratio of ~10^7, μ_{FE} of 37.2 $cm^2 \cdot V^{-1} \cdot s^{-1}$ and a subthreshold swing of 175 $mV \cdot dec^{-1}$. The E-mode operation of the double-gate fluorinated β-Ga_2O_3 MISFETs was achieved under V_{BG} bias of -9 V. The fluorine plasma treatment of β-Ga_2O_3 grants a facile way to achieve the V_{th} modulation of β-Ga_2O_3 FETs and the realization of β-Ga_2O_3-based smart power electronics.

ACKNOWLDEGEMENTS

Research at the U.S. Naval Research Laboratory was supported by the Office of Naval Research. The research at Korea University was supported by the Technology Development Program to Solve Climate Changes of the National Research Foundation funded by the Ministry of Science and ICT (2017M1A2A2087351) and the Korea Institute of Energy Technology Evaluation and Planning (KETEP), granted financial resource from the Ministry of Trade, Industry & Energy, Korea (No. 20172010104830).

Supporting information

Height profile of pristine and fluorinated β-Ga_2O_3 flakes, output characteristics and transfer curves of bottom gated β-Ga_2O_3 MOSFETs before and after the CF_4 plasma treatment (PDF)

REFERENCES

1. Higashiwaki, M.; Sasaki, K.; Murakami, H.; Kumagai, Y.; Koukitu, A.; Kuramata, A.; Masui, T.; Yamakoshi, S., Recent Progress in Ga_2O_3 Power Devices. Semicond. Sci. Technol. **2016**, *31,* 034001.

2. Mastro, M. A.; Kuramata, A.; Calkins, J.; Kim, J.; Ren, F.; Pearton, S., Perspective—Opportunities and Future Directions for Ga_2O_3. ECS J. Solid State Sci. Technol. **2017**, *6,* P356–P359.

3. Pearton, S.; Yang, J.; Cary IV, P. H.; Ren, F.; Kim, J.; Tadjer, M. J.; Mastro, M. A., A Review of β-Ga_2O_3 Materials, Processing, and Devices. Appl. Phys. Rev. **2018**, *5,* 011301.

4. Baliga, B. J., Semiconductors for High□Voltage, Vertical Channel Field□effect Transistors. J. Appl. Phys. **1982**, *53,* 1759–1764.

5. Reese, S. B.; Remo, T.; Green, J.; Zakutayev, A., How Much Will Gallium Oxide Power Electronics Cost?. Joule **2019**, *3,* 903-907

6. Higashiwaki, M.; Sasaki, K.; Kamimura, T.; Hoi Wong, M.; Krishnamurthy, D.; Kuramata, A.; Masui, T.; Yamakoshi, S., Depletion-mode Ga_2O_3 Metal-Oxide-Semiconductor Field-effect Transistors on β-Ga_2O_3 (010) Substrates and Temperature Dependence of their Device Characteristics. Appl. Phys. Lett. **2013**, *103,* 123511.

7. Tadjer, M. J.; Mahadik, N. A.; Wheeler, V. D.; Glaser, E. R.; Ruppalt, L.; Koehler, A. D.; Hobart, K. D.; Eddy, C. R.; Kub, F. J., Editors' Choice Communication—A (001) β-Ga_2O_3 MOSFET with +2.9 V Threshold Voltage and HfO_2 Gate Dielectric. ECS J. Solid State Sci. Technol. **2016**, *5,* P468–P470.

8. Swinnich, E.; Hasan, M. N.; Zeng, K.; Dove, Y.; Singisetti, U.; Mazumder, B.; Seo, J. H., Flexible β□Ga_2O_3 Nanomembrane Schottky Barrier Diodes. Adv. Electron. Mater. **2019**, *5,* 1800714.

9. Barman, S. K.; Huda, M. N., Mechanism Behind the Easy Exfoliation of β-Ga_2O_3 Ultra□Thin Film Along (100) Surface. Phys. Status Solidi RRL **2019**, 1800554.

10. Hwang, W. S.; Verma, A.; Peelaers, H.; Protasenko, V.; Rouvimov, S.; Xing, H.; Seabaugh, A.; Haensch, W.; de Walle, C. V.; Galazka, Z., High-Voltage Field Effect Transistors with Wide-Bandgap β-Ga_2O_3 Nanomembranes. Appl. Phys. Lett. **2014**, *104,* 203111.

11. Kim, J.; Mastro, M. A.; Tadjer, M. J.; Kim, J., Quasi-two-dimensional h-BN/β-Ga_2O_3 Heterostructure Metal–Insulator–Semiconductor Field-effect Transistor. ACS Appl. Mater. Interfaces **2017**, *9,* 21322–21327.

12. Li, Z.; Liu, Y.; Zhang, A.; Liu, Q.; Shen, C.; Wu, F.; Xu, C.; Chen, M.; Fu, H.; Zhou, C., Quasi-two-dimensional β-Ga_2O_3 Field Effect Transistors with Large Drain Current Density and Low Contact Resistance via Controlled Formation of Interfacial Oxygen Vacancies. Nano Res. **2019**, *12,* 143–148.

13. Kim, J.; Mastro, M. A.; Tadjer, M. J.; Kim, J., Heterostructure WSe_2−Ga_2O_3 Junction Field-Effect Transistor for Low-Dimensional High-Power Electronics. ACS Appl. Mater. Interfaces **2018**, *10,* 29724–29729.

14. Hajnal, Z.; Miró, J.; Kiss, G.; Réti, F.; Deák, P.; Herndon, R. C.; Kuperberg, J. M., Role of Oxygen Vacancy Defect States in the n-type Conduction of β-Ga_2O_3. J. Appl. Phys. **1999**, *86,* 3792–3796.

15. Varley, J. B.; Weber, J. R.; Janotti, A.; Van de Walle, C. G., Oxygen vacancies and donor impurities in β-Ga_2O_3. Appl. Phys. Lett., **2010**, *97,* 142106.

16. Ahn, S.; Ren, F.; Kim, J.; Oh, S.; Kim, J.; Mastro, M. A.; Pearton, S., Effect of Front

and Back Gates on β-Ga_2O_3 Nano-Belt Field-Effect Transistors. Appl. Phys. Lett. **2016**, *109,* 062102.

17. Zhou, H.; Maize, K.; Noh, J.; Shakouri, A.; Ye, P. D., Thermodynamic Studies of β-Ga_2O_3 Nanomembrane Field-effect Transistors on a Sapphire Substrate. ACS Omega **2017**, *2,* 7723–7729.

18. Hu, Z.; Nomoto, K.; Li, W.; Zhang, Z.; Tanen, N.; Thieu, Q. T.; Sasaki, K.; Kuramata, A.; Nakamura, T.; Jena, D., Breakdown Mechanism in 1 kA/cm^2 and 960 V E-mode β-Ga_2O_3 Vertical Transistors. Appl. Phys. Lett. **2018**, *113,* 122103.

19. Roy, S.; Gao, Z., Direct-write Fabrication of a Nanoscale Digital Logic Element on a Single Nanowire. Nanotechnology **2010**, *21,* 245306.

20. Chabak, K. D.; Moser, N.; Green, A. J.; Walker Jr, D. E.; Tetlak, S. E.; Heller, E.; Crespo, A.; Fitch, R.; McCandless, J. P.; Leedy, K., Enhancement-mode Ga_2O_3 Wrap-Gate Fin Field-effect Transistors on Native (100) β-Ga_2O_3 Substrate with High Breakdown Voltage. Appl. Phys. Lett. **2016**, *109,* 213501.

21. Chabak, K. D.; McCandless, J. P.; Moser, N. A.; Green, A. J.; Mahalingam, K.; Crespo, A.; Hendricks, N.; Howe, B. M.; Tetlak, S. E.; Leedy, K., Recessed-Gate Enhancement-Mode β-Ga_2O_3 MOSFETs. IEEE Electron Device Lett. **2018**, *39,* 67–70.

22. Wong, M. H.; Nakata, Y.; Kuramata, A.; Yamakoshi, S.; Higashiwaki, M., Enhancement-mode Ga_2O_3 MOSFETs with Si-ion-implanted Source and Drain. Appl. Phys. Express **2017**, *10,* 041101.

23. Zhou, H.; Si, M.; Alghamdi, S.; Qiu, G.; Yang, L.; Peide, D. Y., High-Performance Depletion/Enhancement-mode β-Ga_2O_3 on Insulator (GOOI) Field-Effect Transistors with Record Drain Currents of 600/450 mA/mm. IEEE Electron Device Lett. **2017**, *38,* 103–106.

24. Cai, Y.; Zhou, Y.; Chen, K. J.; Lau, K. M., High-performance Enhancement-mode AlGaN/GaN HEMTs using Fluoride-based Plasma Treatment. IEEE Electron Device Lett.

2005, *26,* 435–437.

25. Cai, Y.; Zhou, Y.; Lau, K. M.; Chen, K. J., Control of Threshold Voltage of AlGaN/GaN HEMTs by Fluoride-based Plasma Treatment: From Depletion Mode to Enhancement Mode. IEEE Trans. Electron Devices **2006**, *53,* 2207–2215.

26. Zaidi, Z.; Lee, K.; Guiney, I.; Qian, H.; Jiang, S.; Wallis, D. J.; Humphreys, C. J.; Houston, P., Enhancement Mode Operation in AlInN/GaN (MIS) HEMTs on Si Substrates using a Fluorine Implant. Semicond. Sci. Technol. **2015**, *30,* 105007.

27. Qian, L. X.; Lai, P. T., Fluorinated InGaZnO Thin-Film Transistor with HfLaO Gate Dielectric. IEEE Electron Device Lett. **2014**, *35,* 363–365.

28. Ruan, D.-B.; Liu, P.-T.; Chiu, Y.-C.; Yu, M.-C.; Gan, K.-J.; Chien, T.-C.; Chen, Y.-H.; Kuo, P.-Y.; Sze, S. M., Performance Improvements of Tungsten and Zinc Doped Indium Oxide Thin Film Transistor by Fluorine based Double Plasma Treatment with a High-K Gate Dielectric. Thin Solid Films **2018**, *665,* 117–122.

29. Yang, J.; Fares, C.; Ren, F.; Sharma, R.; Patrick, E.; Law, M. E.; Pearton, S.; Kuramata, A., Effects of Fluorine Incorporation into β-Ga_2O_3. J. Appl. Phys. **2018**, *123,* 165706.

30. Zhu, Y.; Yu, Q.-K.; Ding, G.-Q.; Xu, X.-G.; Wu, T.-R.; Gong, Q.; Yuan, N.-Y.; Ding, J.-N.; Wang, S.-M.; Xie, X.-M., Raman Enhancement by Graphene-Ga_2O_3 2D Bilayer Film. Nanoscale Res. Lett. **2014**, *9,* 48.

31. Sun, Z.; Yang, L.; Shen, X.; Chen, Z., Anisotropic Raman Spectroscopy of a Single β-Ga_2O_3 Nanobelt. Sci. Bull. **2012**, *57,* 565–568.

32. Reich, S.; Ferrari, A.; Arenal, R.; Loiseau, A.; Bello, I.; Robertson, J., Resonant Raman Scattering in Cubic and Hexagonal Boron Nitride. Phys. Rev. B **2005**, *71,* 205201.

33. Huang, S.; Chen, H.; Chen, K. J., Effects of the Fluorine Plasma Treatment on the Surface Potential and Schottky Barrier Height of $Al_xGa_{1-x}N$/GaN Heterostructures. Appl.

Phys. Lett. **2010**, *96,* 233510.

34. Wang, Y.-H.; Liang, Y. C.; Samudra, G. S.; Huang, C.-F.; Kuo, W.-H.; Lo, G.-Q., The Physical Mechanism on the Threshold Voltage Temperature Stability Improvement for GaN HEMTs with Pre-fluorination Argon Treatment. Appl. Phys. Lett. **2016**, *108,* 233507.

35. SZE, Simon M.; NG, Kwok K., Physics of semiconductor devices. John wiley & sons, 2006.

36. Tang, G.; Kwan, A. M.; Wong, R. K.; Lei, J.; Su, R.; Yao, F.; Lin, Y.; Yu, J.; Tsai, T.; Tuan, H., Digital Integrated Circuits on an E-mode GaN Power HEMT Platform. IEEE Electron Device Lett. **2017**, *38,* 1282–1285.

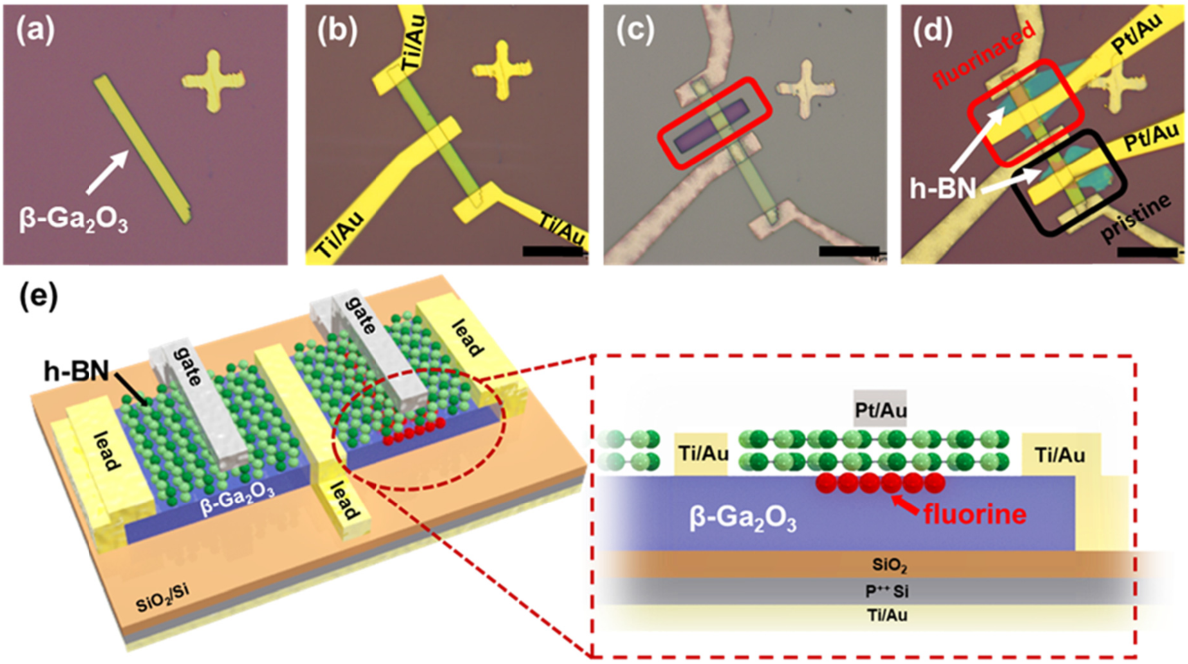

Figure 1 Optical microscope images of each fabrication step of a series of pristine and fluorinated β-Ga_2O_3 MISFETs; (a) β-Ga_2O_3 flake was transferred onto the SiO_2/p^{++}–Si substrate pre-patterned with Ti/Au back-gate electrode (b) Source and drain electrodes were defined on a single β-Ga_2O_3 flake. (c) After the sample was coated with ER, part of the β-Ga_2O_3 flake was opened for remote CF_4 plasma treatment. (d) Two h-BN nanosheets were deposited on each channel and Pt/Au gate electrodes were defined on each channel. The scale bars are 10 μm. (e) Schematic of the series of pristine and fluorinated β-Ga_2O_3 MISFETs with the front (Pt/Au) and back (Ti/Au) gate electrodes.

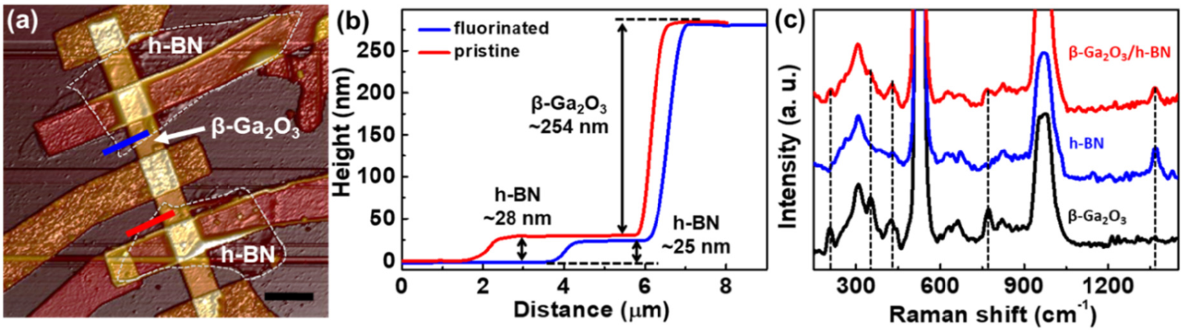

Figure 2 (a) AFM image of the fabricated series of pristine and fluorinated β-Ga_2O_3 MISFETs. The scale bar is 5 μm. (b) Height profile of the β-Ga_2O_3 and multilayer h-BN in both pristine and fluorinated regions. (c) Raman spectra before and after the dry transfer.

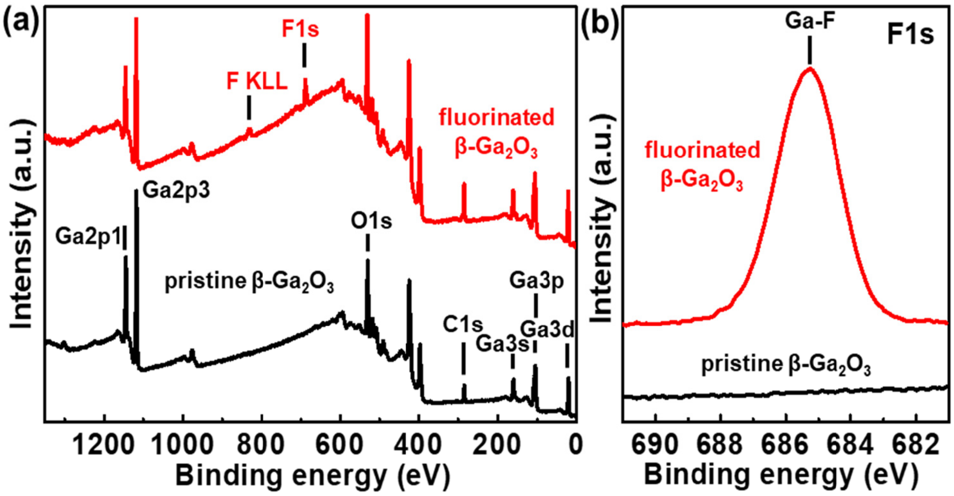

Figure 3 (a) XPS survey scans from the pristine and fluorinated β-Ga_2O_3 surfaces. (b) XPS spectrum of F1s for pristine and fluorinated β-Ga_2O_3

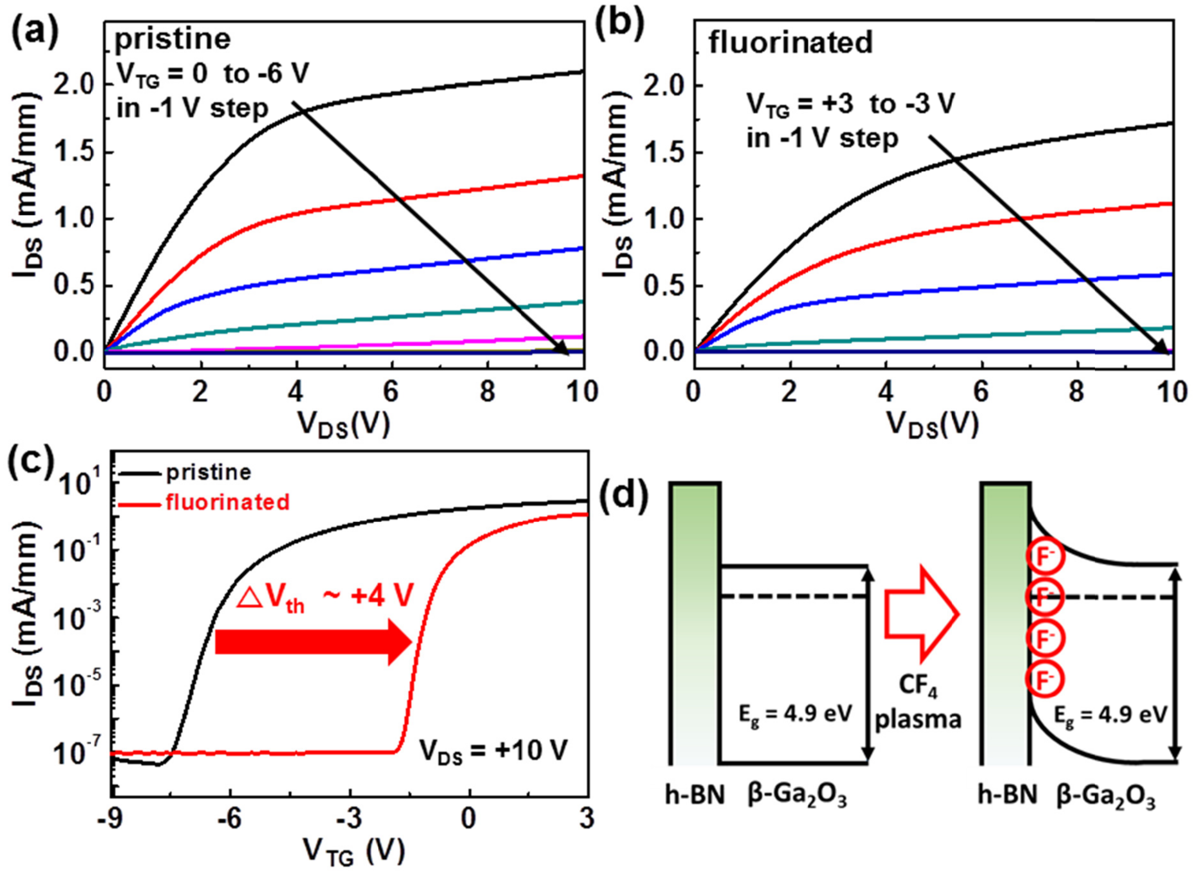

Figure 4 (a–b) I_{DS}–V_{DS} output characteristics of pristine and fluorinated β-Ga_2O_3 MISFETs. (c) Transfer curves of pristine and fluorinated β-Ga_2O_3 MISFETs. (d) Energy-band diagram of a h-BN/ β-Ga_2O_3 flake before and after CF_4 plasma treatment .

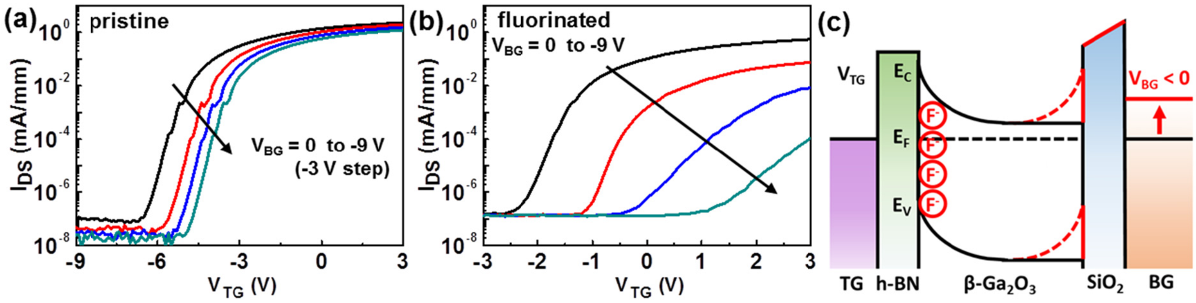

Figure 5 Transfer curves of the double-gated (a) pristine and (b) fluorinated β-Ga_2O_3 MISFETs with varying the back gate (V_{BG}) and the top gate (V_{TG}) at V_{DS}=+10 V (c) the energy band diagram of the fluorinated β-Ga_2O_3 channel under V_{BG}<0 V (note that V_{TG} is not biased).

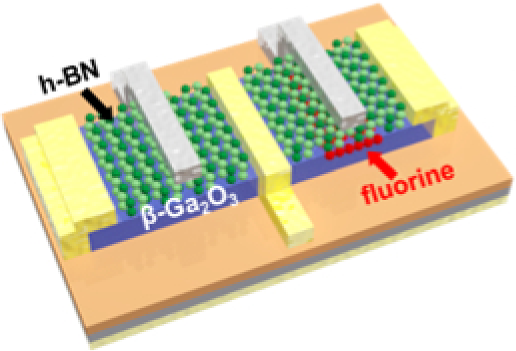
h-BN
β-Ga₂O₃
fluorine

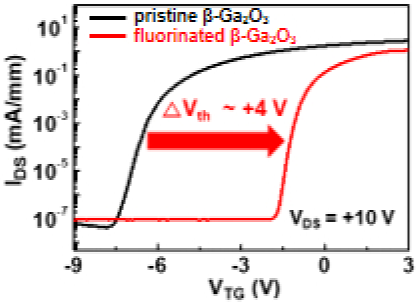
pristine β-Ga₂O₃
fluorinated β-Ga₂O₃
△V_th ~ +4 V
V_DS = +10 V
I_DS (mA/mm)
10¹
10⁻¹
10⁻³
10⁻⁵
10⁻⁷
-9
-6
-3
0
3
V_TG (V)